Research Article Vol. 24, No. 15 / 25 Jul 2016 / OPTICS EXPRESS 16425
Optics EXPRESS

Co-occurrence of circular dichroism and asymmetric transmission in twist nanoslit-nanorod Arrays

YONGKAI WANG, XIAOJING WEN, YU QU, LI WANG, RENGANG WAN, AND ZHONGYUE ZHANG*

School of Physics and Information Technology, Shaanxi Normal University, Xi'an 710062, China
**zyzhang@snnu.edu.cn*

Abstract: Circular dichroism (CD) and asymmetric transmission (AT) are important in the field of negative refractive index media and perfect polarization converters. A large difference between T_{++} and T_{--} in the transmission matrix **T** leads to a large CD effect, whereas a large difference between T_{-+} and T_{+-} leads to a large AT effect. To achieve large CD and AT effects simultaneously, we theoretically analyzed the transmission matrix **T** and proposed the chiral plasmonic nanostructure of twist nanoslit–nanorod arrays (TNNAs) in this study. Results calculated by the finite element method show that, at around resonant wavelengths, the spectra of T_{++} and T_{--} correspondingly present peaks and valleys leading to a large CD effect. Meanwhile one of the spectra for T_{-+} and T_{+-} presents valleys and another presents peaks leading to a large AT effect. More importantly, the magnitude of CD is equivalent to that of AT. In addition, the CD and AT effects strongly depend on the geometric parameters of TNNAs. Overall, these results are useful for designing chiral plasmonic nanostructures with large CD and AT effects.

OCIS codes: (260.2110) Electromagnetic optics; (160.1585) Chiral media; (250.5403) Plasmonics.

References and links

1. G. M. Sherman, "Circular dichroism of long wavelength forms of chlorophyll alpha," Nature **224**(5224), 1108–1110 (1969).
2. P. P. Wei, A. B. Tomter, Å. K. Røhr, K. K. Andersson, and E. I. Solomon, "Circular dichroism and magnetic circular dichroism studies of the active site of p53R2 from human and mouse: iron binding and nature of the biferrous site relative to other ribonucleotide reductases," Biochemistry **45**(47), 14043–14051 (2006).
3. S. M. Kelly, T. J. Jess, and N. C. Price, "How to study proteins by circular dichroism," Biochim. Biophys. Acta **1751**(2), 119–139 (2005).
4. Y. He, G. K. Larsen, W. Ingram, and Y. Zhao, "Tunable three-dimensional helically stacked plasmonic layers on nanosphere monolayers," Nano Lett. **14**(4), 1976–1981 (2014).
5. J. Kaschke, J. K. Gansel, and M. Wegener, "On metamaterial circular polarizers based on metal N-helices," Opt. Express **20**(23), 26012–26020 (2012).
6. S. Droulias and V. Yannopapas, "Broad-band giant circular dichroism in metamaterials of twisted chains of metallic nanoparticles," J. Phys. Chem. C **117**(2), 1130–1135 (2013).
7. C. Menzel, C. Helgert, C. Rockstuhl, E. B. Kley, A. Tünnermann, T. Pertsch, and F. Lederer, "Asymmetric transmission of linearly polarized light at optical metamaterials," Phys. Rev. Lett. **104**(25), 253902 (2010).
8. V. Yannopapas, "One-way photonic band gaps and optical isolation with three-dimensional photonic crystals of low symmetry," Phys. Rev. A **88**(4), 043837 (2013).
9. V. Yannopapas, "Unidirectional Wave Propagation in Low-Symmetric Colloidal Photonic-Crystal Heterostructures," Nanomaterials (Basel) **5**(1), 376–385 (2015).
10. W. Ma, H. Kuang, L. Xu, L. Ding, C. Xu, L. Wang, and N. A. Kotov, "Attomolar DNA detection with chiral nanorod assemblies," Nat. Commun. **4**(2689), 2689 (2013).
11. Y. Mochida, H. Cabral, Y. Miura, F. Albertini, S. Fukushima, K. Osada, N. Nishiyama, and K. Kataoka, "Bundled assembly of helical nanostructures in polymeric micelles loaded with platinum drugs enhancing therapeutic efficiency against pancreatic tumor," ACS Nano **8**(7), 6724–6738 (2014).
12. E. Hendry, T. Carpy, J. Johnston, M. Popland, R. V. Mikhaylovskiy, A. J. Lapthorn, S. M. Kelly, L. D. Barron, N. Gadegaard, and M. Kadodwala, "Ultrasensitive detection and characterization of biomolecules using superchiral fields," Nat. Nanotechnol. **5**(11), 783–787 (2010).

#263579 http://dx.doi.org/10.1364/OE.24.016425
Journal © 2016 Received 20 Apr 2016; revised 24 Jun 2016; accepted 26 Jun 2016; published 12 Jul 2016

Optics EXPRESS

13. B. M. Maoz, R. van der Weegen, Z. Fan, A. O. Govorov, G. Ellestad, N. Berova, E. W. Meijer, and G. Markovich, "Plasmonic chiroptical response of silver nanoparticles interacting with chiral supramolecular assemblies," J. Am. Chem. Soc. **134**(42), 17807–17813 (2012).
14. Y. Zhu, L. Xu, W. Ma, Z. Xu, H. Kuang, L. Wang, and C. Xu, "A one-step homogeneous plasmonic circular dichroism detection of aqueous mercury ions using nucleic acid functionalized gold nanorods," Chem. Commun. (Camb.) **48**(97), 11889–11891 (2012).
15. F. Zhu, X. Li, Y. Li, M. Yan, and S. Liu, "Enantioselective circular dichroism sensing of cysteine and glutathione with gold nanorods," Anal. Chem. **87**(1), 357–361 (2015).
16. Y. Zhao, M. A. Belkin, and A. Alù, "Twisted optical metamaterials for planarized ultrathin broadband circular polarizers," Nat. Commun. **3**(870), 870 (2012).
17. J. B. Pendry, "A chiral route to negative refraction," Science **306**(5700), 1353–1355 (2004).
18. B. Wang, J. Zhou, T. Koschny, and C. M. Soukoulis, "Nonplanar chiral metamaterials with negative index," Appl. Phys. Lett. **94**(15), 151112 (2009).
19. E. Plum, J. Zhou, J. Dong, V. A. Fedotov, T. Koschny, C. M. Soukoulis, and N. I. Zheludev, "Metamaterial with negative index due to chirality," Phys. Rev. B **79**(3), 035407 (2009).
20. V. Yannopapas, "Circular dichroism in planar nonchiral plasmonic metamaterials," Opt. Lett. **34**(5), 632–634 (2009).
21. X. Tian, Y. Fang, and B. Zhang, "Multipolar Fano resonances and Fano-assisted optical activity in silver nanorice heterodimers," ACS Photonics **1**(11), 1156–1164 (2014).
22. T. Cao, C. Wei, L. Mao, and Y. Li, "Extrinsic 2D chirality: giant circular conversion dichroism from a metal-dielectric-metal square array," Sci. Rep. **4**(7442), 7442 (2014).
23. W. X. Huang, Y. Zhang, X. M. Tang, L. S. Cai, J. W. Zhao, L. Zhou, Q. J. Wang, C. P. Huang, and Y. Y. Zhu, "Optical properties of a planar metamaterial with chiral symmetry breaking," Opt. Lett. **36**(17), 3359–3361 (2011).
24. B. K. Canfield, S. Kujala, K. Laiho, K. Jefimovs, J. Turunen, and M. Kauranen, "Chirality arising from small defects in gold nanoparticle arrays," Opt. Express **14**(2), 950–955 (2006).
25. A. S. Schwanecke, V. A. Fedotov, V. V. Khardikov, S. L. Prosvirnin, Y. Chen, and N. I. Zheludev, "Nanostructured metal film with asymmetric optical transmission," Nano Lett. **8**(9), 2940–2943 (2008).
26. R. Singh, E. Plum, C. Menzel, C. Rockstuhl, A. K. Azad, R. A. Cheville, and N. I. Zheludev, "Terahertz metamaterial with asymmetric transmission," Phys. Rev. B **80**(15), 153104 (2009).
27. C. Pan, M. Ren, Q. Li, S. Fan, and J. Xu, "Broadband asymmetric transmission of optical waves from spiral plasmonic metamaterials," Appl. Phys. Lett. **104**(12), 121112 (2014).
28. Y. Wang, J. Deng, G. Wang, T. Fu, Y. Qu, and Z. Zhang, "Plasmonic chirality of L-shaped nanostructure composed of two slices with different thickness," Opt. Express **24**(3), 2307–2317 (2016).
29. Z. Y. Zhang and Y. P. Zhao, "Optical properties of helical Ag nanostructures calculated by discrete dipole approximation method," Appl. Phys. Lett. **90**(22), 221501 (2007).
30. G. K. Larsen, Y. He, J. Wang, and Y. Zhao, "Scalable fabrication of composite Ti/Ag plasmonic helices: controlling morphology and optical activity by tailoring material properties," Adv. Optical Mater. **2**(3), 245–249 (2014).
31. J. Kaschke, L. Blume, L. Wu, M. Thiel, K. Bade, Z. Yang, and M. A. Wegener, "A Helical Metamaterial for Broadband Circular Polarization Conversion," Adv. Optical Mater. **3**(10), 1411–1417 (2015).
32. J. Han, H. Li, Y. Fan, Z. Wei, C. Wu, Y. Cao, and Z. Wang, "An ultrathin twist-structure polarization transformer based on fish-scale metallic wires," Appl. Phys. Lett. **98**(15), 151908 (2011).
33. J. K. Gansel, M. Wegener, S. Burger, and S. Linden, "Gold helix photonic metamaterials: a numerical parameter study," Opt. Express **18**(2), 1059–1069 (2010).
34. C. Pfeiffer, C. Zhang, V. Ray, L. J. Guo, and A. Grbic, "High performance bianisotropic metasurfaces: asymmetric transmission of light," Phys. Rev. Lett. **113**(2), 023902 (2014).
35. L. Wu, Z. Yang, Y. Cheng, M. Zhao, R. Gong, Y. Zheng, and X. Yuan, "Giant asymmetric transmission of circular polarization in layer-by-layer chiral metamaterials," Appl. Phys. Lett. **103**(2), 021903 (2013).
36. L. Wu, Z. Yang, Y. Cheng, Z. Lu, P. Zhang, M. Zhao, R. Gong, X. Yuan, Y. Zheng, and J. Duan, "Electromagnetic manifestation of chirality in layer-by-layer chiral metamaterials," Opt. Express **21**(5), 5239–5246 (2013).
37. C. Huang, Y. Feng, J. Zhao, Z. Wang, and T. Jiang, "Asymmetric electromagnetic wave transmission of linear polarization via polarization conversion through chiral metamaterial structures," Phys. Rev. B **85**(19), 195131 (2012).
38. Y. K. Wang, Y. Qin, and Z. Y. Zhang, "Broadband extraordinary optical transmission through gold diamond-shaped nanohole arrays," IEEE Photonics J. **6**(4), 4801508 (2014).
39. Q. Hong, T. X. Wu, X. Zhu, R. Lu, and S. T. Wu, "Extraordinarily high-contrast and wide-view liquid-crystal displays," Appl. Phys. Lett. **86**(12), 121107 (2005).
40. P. B. Johnson and R. W. Christy, "Optical constants of the noble metals," Phys. Rev. B **6**(12), 4370–4379 (1972).
41. Q. Li and Z. Zhang, "Bonding and anti-bonding modes of plasmon coupling effects in TiO2-Ag core-shell dimers," Sci. Rep. **6**(19433), 19433 (2016).
42. X. Yin, M. Schäferling, B. Metzger, and H. Giessen, "Interpreting chiral nanophotonic spectra: the plasmonic Born-Kuhn model," Nano Lett. **13**(12), 6238–6243 (2013).

Optics EXPRESS

43. K. D. Osberg, N. Harris, T. Ozel, J. C. Ku, G. C. Schatz, and C. A. Mirkin, "Systematic study of antibonding modes in gold nanorod dimers and trimers," Nano Lett. **14**(12), 6949–6954 (2014).

1. Introduction

Chiral structures are ones that cannot be made to coincide with their mirror images [1–3]. These structures show interesting optical chirality, such as circular dichroism (CD) and asymmetric transmission (AT) effects. The CD effect is the transmission intensity difference between right-hand circular polarized (RCP, +) light and left-hand circular polarized (LCP, –) light [4–6]. The AT effect is defined as the difference in the conversion of linearly and circularly polarized light into opposite polarized light [7–9]. Owing to the strong interaction between light and noble metals, artificial chiral plasmonic nanostructures (ACPNs) are extensively studied in biological monitoring [10–12], analytical chemistry [13–15], circular polarization conversion [16], and negative refractive index media [17–19].

Recently, many researchers have proposed different ACPNs to produce chirality and explore the reason for chirality. For plasmonic nanostructures, 2D achiral plasmonic nanostructures can achieve a chiral response under oblique excitation [20–22]. However, 2D monolayer ACPNs can achieve CD [23, 24] or AT effects [25–27] under normal excitation. Three dimensional (3D) helical ACPNs show strong CD [28–30] or AT [31–33], which is due the introduction of spatial asymmetry in ACPNs. However, these ACPNs, such as layer-by-layer ACPNs prepared by multiple-steps electron beam lithography (EBL) cannot achieve strong CD and circular AT effects simultaneously [30, 34]. The circular AT is achieved under the condition of $\left|t_{+-}\right| \neq \left|t_{-+}\right| \cap t_{++} = t_{--}$, at which $\mathrm{CD} = \left|t_{++}\right|^2 - \left|t_{--}\right|^2 = 0$ [35].

Simultaneously achieving CD and AT is important in the field of negative refractive index media [18] and perfect polarization converters [36]. However, at the resonant wavelength of usual 2D and 3D ACPNs, T_{++} and T_{--} consistently present valleys limiting the magnitude of the CD effect, meanwhile T_{-+} and T_{+-} consistently present peaks limiting the magnitude of the circular AT effect [33]. The magnitudes of T_{-+} and T_{+-} are also weaker than those of T_{++} and T_{--}, respectively, which limits circular polarization conversion.

In this paper, we designed a type of chiral metamaterial nanostructure on the basis of theoretical analysis. The fundamental difference between the previous ACPNs and our designed ACPNs is that our designed ACPNs can simultaneously achieve CD and AT effects. The chiral response of twist nanoslit–nanorod arrays (TNNAs) was investigated by finite element method (FEM) to verify the theoretical prediction. Experimentally, the TNNAs can be prepared by EBL method. FEM calculation results show that the TNNAs can achieve large CD and AT effects simultaneously. The effects of the rotation angle of the nanorod relative to the nanoslit, the length of the nanorod, and the separation between the nanoslit and the nanorod on the CD and AT effects were also studied.

2. Theoretical analysis

Given the incident plane wave propagation along the + *z* direction, the Jones matrix $\mathbf{T}_{\mathrm{circ}}$ of circular polarization [33, 34] is described as

$$\mathbf{T}_{\mathbf{circ}}^{+z} = \frac{1}{2}\begin{pmatrix} t_{xx}+t_{yy}+i(t_{xy}-t_{yx}) & t_{xx}-t_{yy}-i(t_{xy}+t_{yx}) \\ t_{xx}-t_{yy}+i(t_{xy}+t_{yx}) & t_{xx}+t_{yy}-i(t_{xy}-t_{yx}) \end{pmatrix} = \begin{pmatrix} t_{++} & t_{+-} \\ t_{-+} & t_{--} \end{pmatrix} . \qquad (1)$$

We use *x*, *y*, + , and – to describe the polarized states of linearly *x*-polarized, linearly *y*-polarized, RCP light, and LCP light, respectively. $\mathrm{Im}(t_{xx})$ and $\mathrm{Re}(t_{xx})$ represent the real part and imaginary part of t_{xx}, respectively. The CD of the circularly polarized light is usually defined as

Optics EXPRESS

$$\mathbf{CD}^{+z} = \mathbf{T}_{++} - \mathbf{T}_{--} = \left|\boldsymbol{t}_{++}\right|^2 - \left|\boldsymbol{t}_{--}\right|^2 = \left[\mathbf{Im}(\boldsymbol{t}_{xx}) + \mathbf{Im}(\boldsymbol{t}_{yy})\right]\left[\mathbf{Re}(\boldsymbol{t}_{xy}) - \mathbf{Re}(\boldsymbol{t}_{yx})\right] - \left[\mathbf{Re}(\boldsymbol{t}_{xx}) + \mathbf{Re}(\boldsymbol{t}_{yy})\right]\left[\mathbf{Im}(\boldsymbol{t}_{xy}) - \mathbf{Im}(\boldsymbol{t}_{yx})\right]. \quad (2)$$

The AT of the circularly polarized light is defined as

$$\Delta_{\mathbf{circ}}^{+z} = \mathbf{T}_{-+} - \mathbf{T}_{+-} = \left|\boldsymbol{t}_{-+}\right|^2 - \left|\boldsymbol{t}_{+-}\right|^2 = \left[\mathbf{Im}(\boldsymbol{t}_{xx}) - \mathbf{Im}(\boldsymbol{t}_{yy})\right]\left[\mathbf{Re}(\boldsymbol{t}_{xy}) + \mathbf{Re}(\boldsymbol{t}_{yx})\right] - \left[\mathbf{Re}(\boldsymbol{t}_{xx}) - \mathbf{Re}(\boldsymbol{t}_{yy})\right]\left[\mathbf{Im}(\boldsymbol{t}_{xy}) + \mathbf{Im}(\boldsymbol{t}_{yx})\right]. \quad (3)$$

For traditional structures, no special relationships usually exist among the elements of $\mathbf{T}_{\text{circ}}$ [7, 33, 36]. Simultaneously achieving large CD and AT effects is difficult. According to Eqs. (2) and (3), large CD^{+z} and large $\Delta_{\mathbf{circ}}^{+z}$ can be achieved simultaneously by satisfying the condition of

$$\boldsymbol{t}_{xx} = \boldsymbol{t}_{xy} = 0. \quad (4)$$

We propose the composed structure of nanoslits and nanorods to satisfy Eq. (4). According to previous literature [38], extraordinary optical transmission of nanoslits only occurs under linear polarization perpendicular to the slits. The Jones matrix of nanoslit arrays on *x* direction ($\mathbf{T}_{\mathbf{lin\text{-}Slit}}^{+z}$) can be written as

$$\mathbf{T}_{\mathbf{lin\text{-}Slit}}^{+z} = \begin{pmatrix} 0 & 0 \\ 0 & t_s \end{pmatrix}, \quad (5)$$

where t_s is the complex transmission coefficient, which is a function of the incident light frequency. While it can be seen that for the nanoslit array $\boldsymbol{t}_{xx} = \boldsymbol{t}_{xy} = 0$, they are achiral. Introducing nanorod arrays offers a generic Jones matrix, which can break the mirror symmetry of the nanoslit and render the combined structure chiral. The Jones matrix of nanorod arrays ($\mathbf{T}_{\mathbf{lin\text{-}Nano}}^{+z}$) can be written as

$$\mathbf{T}_{\mathbf{lin\text{-}Nano}}^{+z} = \begin{pmatrix} a & b \\ c & d \end{pmatrix}, \quad (6)$$

where *a*, *b*, *c*, and *d* are the complex transmission coefficients, which are functions of incident light frequency. When the reflections between naoslits and nanorods are negligible, the Jones matrix of the composed slit-rod system would be constructed as the multiplication of the matrices belonging to the individual components [39]. The Jones matrix of the composition of ACPNs ($\mathbf{T}_{\mathbf{lin\text{-}ACPN}}^{+z}$) can be written as

$$\mathbf{T}_{\mathbf{lin\text{-}ACPN}}^{+z} = \mathbf{T}_{\mathbf{lin\text{-}Slit}}^{+z} * \mathbf{T}_{\mathbf{lin\text{-}Nano}}^{+z} = \begin{pmatrix} 0 & 0 \\ 0 & t_s \end{pmatrix}\begin{pmatrix} a & b \\ c & d \end{pmatrix} = \begin{pmatrix} 0 & 0 \\ ct_s & dt_s \end{pmatrix}. \quad (7)$$

In accordance with Eq. (4), the condition of $\boldsymbol{t}_{xx} = \boldsymbol{t}_{xy} = 0$ show that TNNAs will produce CD and AT simultaneously. The CD and AT can be written as

$$\begin{aligned} \mathbf{CD}^{+z} &= \left[\mathbf{Im}(\boldsymbol{t}_{xx}) + \mathbf{Im}(\boldsymbol{t}_{yy})\right]\left[\mathbf{Re}(\boldsymbol{t}_{xy}) - \mathbf{Re}(\boldsymbol{t}_{yx})\right] - \left[\mathbf{Re}(\boldsymbol{t}_{xx}) + \mathbf{Re}(\boldsymbol{t}_{yy})\right]\left[\mathbf{Im}(\boldsymbol{t}_{xy}) - \mathbf{Im}(\boldsymbol{t}_{yx})\right] \\ &= \left[\mathbf{Im}(0) + \mathbf{Im}(dt_s)\right]\left[\mathbf{Re}(0) - \mathbf{Re}(ct_s)\right] - \left[\mathbf{Re}(0) + \mathbf{Re}(dt_s)\right]\left[\mathbf{Im}(0) - \mathbf{Im}(ct_s)\right] \\ &= -\mathbf{Im}(dt_s)\mathbf{Re}(ct_s) + \mathbf{Re}(dt_s)\mathbf{Im}(ct_s), \end{aligned} \quad (8)$$

and

Optics EXPRESS

$$\begin{aligned}\Delta_{\mathrm{circ}}^{+z} &= \left[\mathrm{Im}(t_{xx}) - \mathrm{Im}(t_{yy})\right]\left[\mathrm{Re}(t_{xy}) + \mathrm{Re}(t_{yx})\right] - \left[\mathrm{Re}(t_{xx}) - \mathrm{Re}(t_{yy})\right]\left[\mathrm{Im}(t_{xy}) + \mathrm{Im}(t_{yx})\right] \\ &= \left[\mathrm{Im}(0) - \mathrm{Im}(dt_{\mathrm{s}})\right]\left[\mathrm{Re}(0) + \mathrm{Re}(ct_{\mathrm{s}})\right] - \left[\mathrm{Re}(0) - \mathrm{Re}(dt_{\mathrm{s}})\right]\left[\mathrm{Im}(0) + \mathrm{Im}(ct_{\mathrm{s}})\right] \quad (9) \\ &= -\mathrm{Im}(dt_{\mathrm{s}})\mathrm{Re}(ct_{\mathrm{s}}) + \mathrm{Re}(dt_{\mathrm{s}})\mathrm{Im}(ct_{\mathrm{s}}).\end{aligned}$$

When light illuminates the proposed structure backward, the Jones matrix $\mathbf{T}_{\mathrm{lin\text{-}ACPN}}^{-z}$ can be written as

$$\mathbf{T}_{\mathrm{lin-ACPN}}^{-z} = \mathbf{T}_{\mathrm{lin-Nano}}^{-z} * \mathbf{T}_{\mathrm{lin-Slit}}^{-z} = \begin{pmatrix} a & -c \\ -b & d \end{pmatrix}\begin{pmatrix} 0 & -0 \\ -0 & t_{\mathrm{s}} \end{pmatrix} = \begin{pmatrix} 0 & -ct_{\mathrm{s}} \\ 0 & dt_{\mathrm{s}} \end{pmatrix}. \quad (10)$$

Thus,

$$\begin{aligned}\mathbf{CD}^{-z} &= \left[\mathrm{Im}(t_{xx}) + \mathrm{Im}(t_{yy})\right]\left[\mathrm{Re}(t_{xy}) - \mathrm{Re}(t_{yx})\right] - \left[\mathrm{Re}(t_{xx}) + \mathrm{Re}(t_{yy})\right]\left[\mathrm{Im}(t_{xy}) - \mathrm{Im}(t_{yx})\right] \\ &= \left[\mathrm{Im}(0) + \mathrm{Im}(dt_{\mathrm{s}})\right]\left[\mathrm{Re}(-ct_{\mathrm{s}}) - \mathrm{Re}(0)\right] - \left[\mathrm{Re}(0) + \mathrm{Re}(dt_{\mathrm{s}})\right]\left[\mathrm{Im}(-ct_{\mathrm{s}}) - \mathrm{Im}(0)\right] \quad (11) \\ &= -\mathrm{Im}(dt_{\mathrm{s}})\mathrm{Re}(ct_{\mathrm{s}}) + \mathrm{Re}(dt_{\mathrm{s}})\mathrm{Im}(ct_{\mathrm{s}}) = \mathbf{CD}^{+z},\end{aligned}$$

and

$$\begin{aligned}\Delta_{\mathrm{circ}}^{-z} &= \left[\mathrm{Im}(t_{xx}) - \mathrm{Im}(t_{yy})\right]\left[\mathrm{Re}(t_{xy}) + \mathrm{Re}(t_{yx})\right] - \left[\mathrm{Re}(t_{xx}) - \mathrm{Re}(t_{yy})\right]\left[\mathrm{Im}(t_{xy}) + \mathrm{Im}(t_{yx})\right] \\ &= \left[\mathrm{Im}(0) - \mathrm{Im}(dt_{\mathrm{s}})\right]\left[\mathrm{Re}(-ct_{\mathrm{s}}) + \mathrm{Re}(0)\right] - \left[\mathrm{Re}(0) - \mathrm{Re}(dt_{\mathrm{s}})\right]\left[\mathrm{Im}(-ct_{\mathrm{s}}) + \mathrm{Im}(0)\right] \\ &= \mathrm{Im}(dt_{\mathrm{s}})\mathrm{Re}(ct_{\mathrm{s}}) - \mathrm{Re}(dt_{\mathrm{s}})\mathrm{Im}(ct_{\mathrm{s}}) = -\Delta_{\mathrm{circ}}^{+z}.\end{aligned}$$

Equations (11) and (12) show that when light is incident from the $-z$ direction, the CD is the same as that incident from the $+z$ direction, whereas the AT effect is the opposite of that incident from the $+z$ direction. Therefore, TNNAs produce $\left|\mathbf{CD}^{+z}\right| = \left|\mathbf{CD}^{-z}\right| = \left|\Delta_{\mathrm{circ}}^{+z}\right| = \left|\Delta_{\mathrm{circ}}^{-z}\right|$ simultaneously.

Figure 1 shows the proposed TNNAs. The arrays and cell of the TNNAs are shown in Figs. 1(a) and 1(b), respectively. The nanoslits and nanorods are gold, and their frequency dependent permittivities are obtained from Ref. 40. The nanoslits (yellow) and nanorods (yellow) are separated by a SiO_2 layer (blue) with a refractive index of 1.45 and thickness g. The periods of the TNNAs are 1000 nm and 700 nm in the x and y directions, respectively. The height and width of the nanoslits are 100 nm each. The nanorods are located below the nanoslits. The length, width, and height of the nanorods are L, 60 nm, and 60 nm, respectively. The twist angle between the nanoslits and nanorods is α, as shown in the inset in Fig. 1. Incident RCP (aqua circle-arrow) and LCP (pink circle-arrow) light illuminates normally to the structure and can be partially converted into opposite handedness. The solid black arrows labeled by k indicate the directions of wave vectors, which are oriented along the + z or –z direction. FEM software COMSOL Multiphysics is used to calculate the transmittance of the TNNAs.

Optics EXPRESS

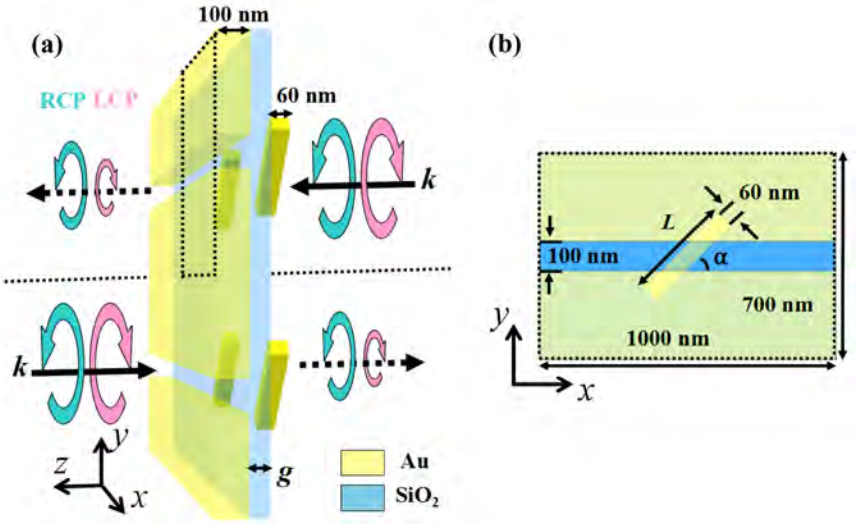

Fig. 1. (a) Schematic of TNNAs with g = 60 nm, L = 360 nm, and α = 45°. (b) Its unit cell with the associated geometric features.

3. Results and discussion

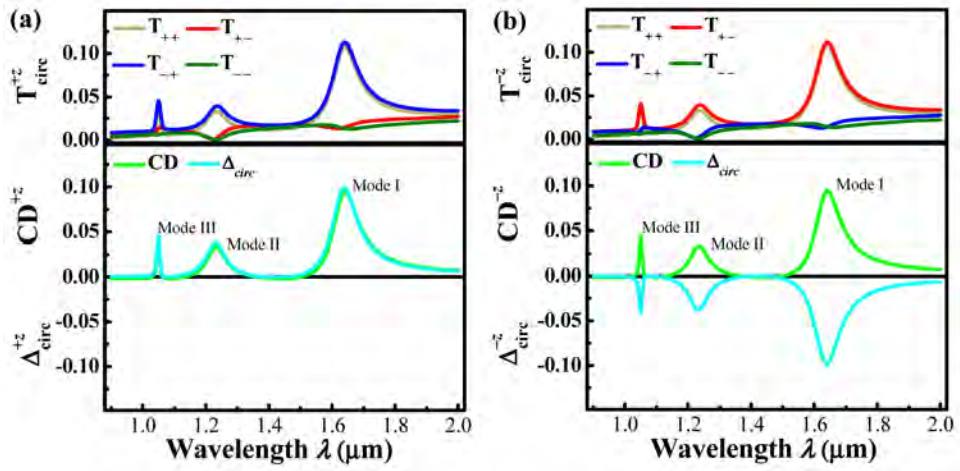

Fig. 2. Simulated $(\mathbf{T})_{circ}$ matrix, CD spectrum, and AT spectrum of TNNAs for + z-direction light excitation (a) and –z-direction light excitation (b). The three resonances are labeled mode I, II, and III.

Figure 2(a) shows the $\mathbf{T}_{circ}^{+z}$, CD^{+z}, and Δ_{circ}^{+z} of TNNAs with g = 60 nm, L = 360 nm, and α = 45°. For the transmitted spectra of T_{++} ($|t_{++}|^2$), T_{+-} ($|t_{+-}|^2$), T_{-+} ($|t_{-+}|^2$), and T_{--} ($|t_{--}|^2$), obvious peaks or valleys are observed at resonance wavelengths λ_I = 1.64 μm, λ_{II} = 1.23 μm, and λ_{III} = 1.05 μm. For simplicity, we divide the resonance modes into modes I, II, and III. At around resonance wavelengths, the spectra of T_{++} and T_{--} correspondingly present peaks and valleys leading to a large CD effect, whereas the spectra of T_{+-} and T_{-+} correspondingly present valleys and peaks leading to a large AT effect. The spectrum of CD is coincident with that of AT. Figure 2(b) shows the $\mathbf{T}_{circ}^{-z}$, CD^{-z}, and Δ_{circ}^{-z} of the TNNAs with the same structural parameters as those in Fig. 2(a). T_{++} and T_{--} are the same as those in Fig. 2(a), which is consistent with Eq. (11). T_{+-} and T_{-+} are exchanged with respect to Fig. 2(a), which

Optics EXPRESS

is consistent with Eq. (12). Under the excitation of LCP light, the magnitude of T_{+-} (transmittance of RCP light) is larger than that of T_{--} (transmittance of LCP light), which achieves a large converter.

The normalized charge distributions of the nanoslit (lower surface) and the nanorod (upper surface) at λ_I = 1.64 μm, λ_{II} = 1.23 μm, and λ_{III} = 1.05 μm are calculated to investigate the origin of the modes in Fig. 2, as shown in Fig. 3. The red color indicates positive charge, and the blue color indicates negative charge. Figures 3(a), 3(d), and 3(g) show the normalized charge distributions of the nanoslit. The magenta solid arrows represent the equivalent electric dipole moments of nanoslits. Figures 3(b), 3(e), and 3(h) show the normalized charge distributions of the nanorod. The charges mainly distribute on the two ends of the nanorod. The green arrows represent the equivalent electric dipole moments of nanorods.

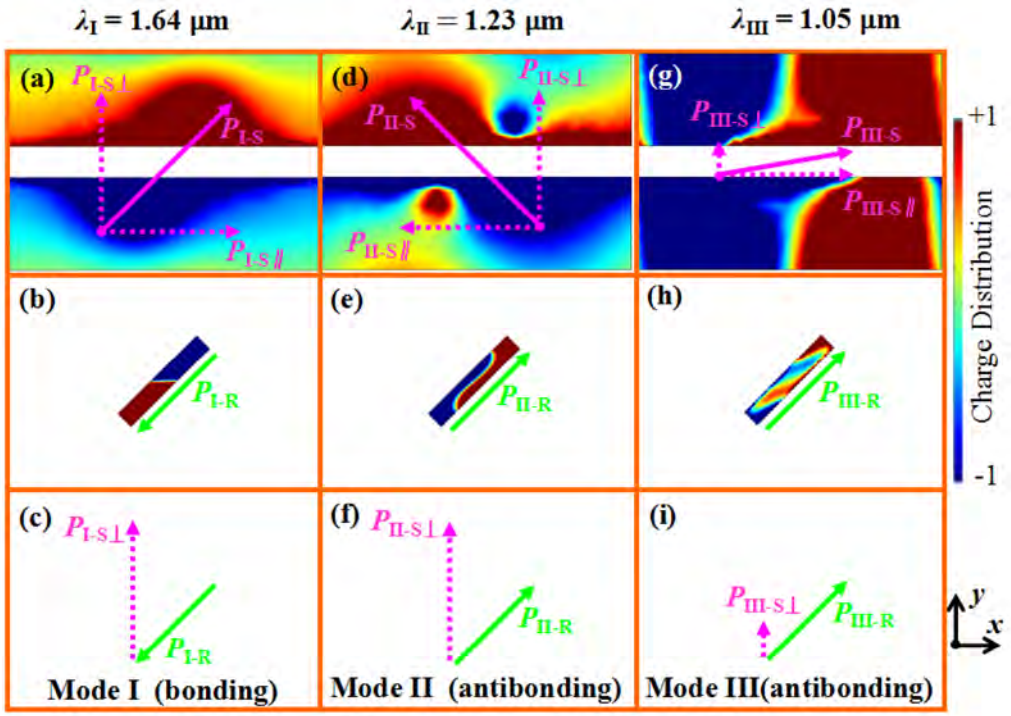

Fig. 3. The charge distributions of (a, d, and g) nanoslits and (b, e, and h) nanorods. (c, f, and i) Born-Kuhn modes of TNNAs for RCP at three modes under –z-direction light excitation.

At λ_I = 1.64 μm, tilted effective dipole $P_{I\text{-}S}$ appears around the slit. $P_{I\text{-}S}$ can be decomposed into $P_{I\text{-}S\perp}$ and $P_{I\text{-}S\parallel}$. The decomposition can be performed for each mode. $P_{I\text{-}S\perp}$ is perpendicular to the slit, which contributes to the transmission of energy through the slit [38]. As shown in Fig. 3(c), $P_{I\text{-}S\perp}$ and $P_{I\text{-}R}$ form a bonding mode in the Born–Kuhn oscillator model [41, 42]. At λ_{II} = 1.23 μm, effective dipole electron oscillation $P_{II\text{-}S}$ is also tilted around the slit. $P_{II\text{-}S\perp}$ is perpendicular to the slit. As shown in Fig. 3(f), $P_{II\text{-}S\perp}$ and $P_{II\text{-}R}$ form an antibonding mode in the Born–Kuhn oscillator model [42]. At λ_{III} = 1.05 μm [Fig. 3(g)], except the region around the slit, a large electric field distributes along the line perpendicular to the slit, which shows that λ_{III} = 1.05 μm is attributed to the electrons oscillating in the direction perpendicular to the slit. In the region around the slit, effective dipole $P_{III\text{-}S}$ exhibits a smaller tilted angle related to the slit than those shown in Figs. 3(a) and 3(d). As shown in Fig. 3(i), $P_{III\text{-}S\perp}$ and $P_{III\text{-}R}$ form an antibonding mode.

We vary the thickness of SiO_2 to investigate the influences of the coupling between nanoslit and nanorod on the CD and AT effects of TNNAs. Figure 4(a) shows the simulated

Optics EXPRESS

CD^{-z} and Δ_{circ}^{-z} spectra of different thickness g with fixed L = 360 nm and α = 45°. Modes I, II, and III are observed in CD^{-z} and Δ_{circ}^{-z} spectra with different thickness g. Mode I blue shifts with an increase in g. Modes II and III red shift as g increases. Given that mode I is ascribed to the bonding mode between $P_{I\text{-}S\perp}$ and $P_{I\text{-}R}$, attraction is presented between $P_{I\text{-}S\perp}$ and $P_{I\text{-}R}$. An increase in g will decrease the attraction between them, leading to a decrease in the equivalent electric dipole moments and the blue shift of the resonant wavelength [43]. On the contrary, modes II and III are attributed to the antibonding mode between the electron oscillations around the slit and on the nanorod; this finding indicates that repulsion exists between them. An increase in g will decrease the repulsion between them, leading to an increase in the equivalent electric dipole moments and the red shift of the resonant wavelength [43].

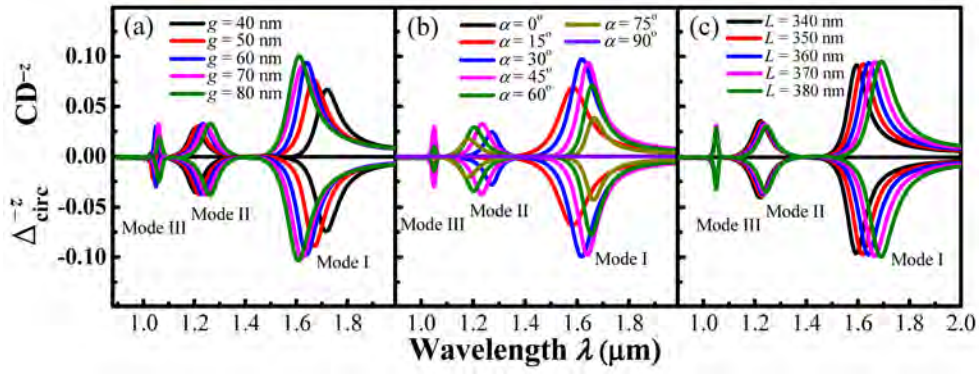

Fig. 4. CD^{-z} and Δ_{circ}^{-z} spectra of TNNAs with different (a) thickness g, (b) angle α, and (c) length L.

We show the simulated CD^{-z} and Δ_{circ}^{-z} spectra of different angle α with fixed L = 360 nm and g = 60 nm in Fig. 4(b) to investigate the effects of angle α on CD and AT. Given α = 0° and 90°, TNNA is achiral, and the three peaks disappear. When α is increased from 15° to 75°, modes I and III red shift, whereas mode II blue shifts. With an increase in α, the component of $P_{I\text{-}S\perp}$ increases, thereby resulting in the red shift of mode I. On the contrary, the component of $P_{II\text{-}S\perp}$ decreases as α increases, which results in the blue shift of mode II. The component of $P_{III\text{-}S\perp}$ increases as α increases, which results in the red shift of mode III.

We also present the simulated CD^{-z} and Δ_{circ}^{-z} spectra of different length L with fixed g = 60 nm and α = 45° in Fig. 4(c) to investigate the effects of length L on CD and AT. The three modes are present in CD^{-z} and Δ_{circ}^{-z} spectra, and all red shift with an increase in L. With an increase in L, the equivalent electric dipole moments on the rod and around the slit increase, resulting in the red shift of the three modes.

4. Conclusions

In this study, we present TNNAs comprising nanoslits and twist nanorods to achieve CD and AT effects simultaneously by analyzing the transmission matrix. The transmission properties of the TNNAs are calculated by FEM. The results show that at resonant wavelengths, the spectra of T_{++} and T_{--} correspondingly present peaks and valleys leading to a large CD effect, meanwhile one of the spectra for T_{-+} and T_{+-} presents valleys and another presents peaks leading to a large AT effect. The magnitude of CD is equivalent to that of AT. When light illuminates the proposed structure backward, the magnitude of T_{+-} is stronger than that of T_{--}, which achieves a large converter. The CD and AT effects strongly depend on the geometric parameters of the TNNAs. Overall, these results are useful for designing negative refractive

Optics EXPRESS

index media and perfect polarization converters. Furthermore, the method of designing nanostructures based on an analysis of the transmission matrix can be employed in negative refractive index media and perfect polarization converters.

Funding

National Natural Science Foundation of China (61575117); Fundamental Research Funds for the Central Universities of Ministry of Education of China (GK201601008); Excellent Doctor Degree Dissertation of Shaanxi Normal University (X2014YB08).